Hindawi Publishing Corporation
Journal of Thermodynamics
Volume 2012, Article ID 725142, 17 pages
doi:10.1155/2012/725142

Research Article

Thermo-Diffusion and Diffusion-Thermo Effects on MHD Free Convective Heat and Mass Transfer from a Sphere Embedded in a Non-Darcian Porous Medium

B. Vasu,[1] V. R. Prasad,[1] and O. Anwar Bég[2]

[1] *Department of Mathematics, Madanapalle Institute of Technology and Science, Madanapalle 517325, India*
[2] *Department of Engineering and Mathematics, Sheffield Hallam University, Room 4112, Sheaf Building, Sheffield S1 1WB, UK*

Correspondence should be addressed to B. Vasu, bvsmaths1@gmail.com

Received 30 March 2012; Revised 11 May 2012; Accepted 12 May 2012

Academic Editor: Mohammad Al-Nimr

The problem of combined heat and mass transfer by natural convection over a sphere in a homogenous non-Darcian porous medium subjected to uniform magnetic field is numerically studied, taking Soret/Dufour effects into account. The coupled, steady, and laminar partial differential conservation equations of mass, momentum, energy, and species diffusion are normalized with appropriate transformations. The resulting well-posed two-point boundary value problem is solved using the well-tested, extensively validated Keller-Box implicit finite difference method, with physically realistic boundary conditions. A parametric study of the influence of Soret number (Sr), Dufour number (Du), Forchheimer parameter (Λ), Darcy parameter (Da), buoyancy ratio parameter (N), Prandtl number (Pr), Schmidt number (Sc), magnetohydrodynamic body force parameter (M), wall transpiration (f_w) is the blowing/suction parameter, and streamwise variable (ξ) on velocity, temperature, and concentration function evolution in the boundary layer regime is presented. Shear stress, Nusselt number, and Sherwood number distributions are also computed. Applications of the study arise in hydromagnetic flow control of conducting transport in packed beds, magnetic materials processing, geophysical energy systems, and magnetohydrodynamic chromatography technology.

1. Introduction

Magnetohydrodynamic transport phenomena arise in numerous branches of modern chemical engineering. These include crystal magnetic damping control [1], hydromagnetic chromatography [2], conducting flows in trickle-bed reactors [3], and enhanced magnetic filtration control [4]. Numerous studies of both an experimental and numerical nature have been communicated regarding magnetohydrodynamic flow in chemical engineering. In general, in such flows, the Lorentz electromagnetic force arises as a result of the interaction between the magnetic field and the electrical current. This latter is generated hydrodynamically by the bulk flow of the conducting liquid phase. In porous media applications such as packed beds, to sustain a given flow rate of the electrically conducting liquid in the bed, the pressure drop and the liquid holdup will be increased under magnetohydrodynamic conditions compared with the case of nonconducting fluids. In crystal growth applications in porous media, the external magnetic field imposed has been successfully exploited to suppress unsteady flow and also reduce composition nonuniformity. The most extensively studied flows involve static magnetic fields which may be aligned (for which magnetic boundary layers arise) [5, 6], transversal [7–11], radial [12, 13], inclined [14, 15] and so forth. Researchers have also considered the use of rotating magnetic fields to control convection in the solution zone during crystal growth by, for example, the traveling heater method (THM). A wide variety of mathematical models have been employed in simulating magnetohydrodynamic transport in both fluid and also porous media regimes. Rudariah et al. [16] obtained analytical solutions for Hartmann-Couette flow in a porous regime, showing that for mercury flowing over a long permeable channel of width 0.7 cm, the effect of magnetic field (of strength 0.25 Web/m^2, for which Hartmann number = 8.8) in the presence of a porous wall (of permeability = 5×10^{-6} Darcy) is to retard the mass flow and to increase the friction factor relative to the corresponding

quantities for nonmagnetic flow. They further identified that transition to turbulence occurs at a higher Reynolds number owing to the presence of a magnetic field. Lioubashevski et al. [17] investigated the effect of a static homogeneous magnetic field orientated parallel to the planar electrode surface using a hydrodynamic boundary layer formation and equivalent mass transfer model for a semiinfinite electrode, showing that there is a decrease of the boundary layer thickness with increasing magnetic field strength or reagent bulk concentration. Boum and Alemany [18] studied mass transfer processes in an electrochemical system under an applied external magnetic field, studying in particular the magnetically induced flow of electrolyte in a short duct. Fahidy [19] employed an approximate method for the estimation of the mean velocity and the root mean square velocity in the natural-convective diffusion boundary layer under weak magnetic field, examining in detail the case of a vertical solid surface where the electric and magnetic field are horizontal and mutually transverse. Al-Nimr and Hader [20] obtained closed form solutions for fully developed hydromagnetic free convection flow in open-ended vertical porous channels using a superposition method, for four different boundary conditions. McWhirter et al. [21] presented an analytical model for magnetohydrodynamic porous medium flow, simulating the regime as a packed bed of uniform spheres. They considered two particular cases—an infinite packed bed and a finite packed bed including wall effects, the latter being modeled with a two-zone porosity model, with a higher porosity wall region inserted between the solid wall and the lower porosity core region. Dahikar and Sonolikar [22] studied experimentally the hydromagnetic flow in scaled magnetically assisted circulating fluidized bed, with a circular cross-section, showing that magnetic field strongly influences fluidization phenomenon and accelerates the transition towards much denser suspension of the fluidized bed. Alchaar et al. [23] studied the stability of free convection in a porous regime under transverse magnetic field using a CFD(computational fluid dynamics) approach. Mansour et al. [24] used a power series expansion method to assess the steady convective heat and mass transfer in micropolar conducting flow on a circular cylinder maintained at uniform heat and mass flux. Postelnicu [25] conducted a theoretical study of magnetohydrodynamic free convection heat and mass transfer from a vertical surface in a porous medium, incorporating Dufour and Soret diffusion effects, showing that increasing magnetic field elevates the local Nusselt and Sherwood numbers. The above studies have not considered the combined thermal convection and mass diffusion in magnetohydrodynamic boundary layer flow from a sphere in a porous medium, despite the importance of such a problem in filtration engineering and materials processing. It is therefore proposed to study this problem in the present paper. Furthermore, the medium is simulated to include non-Darcian and variable porosity effects with blowing/suction also included for the sphere surface. A well-tested implicit finite difference procedure, the Keller-box method is used to solve the transformed boundary layer equations. A detailed discussion of the effects of thermophysical parameters on flow variables is provided.

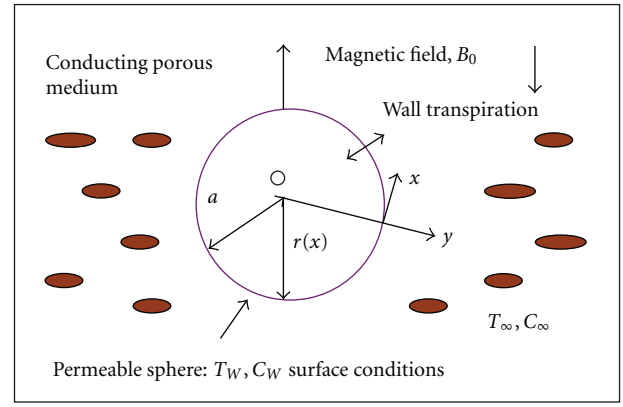

Figure 1: Physical model.

2. Mathematical Model

We consider the steady, laminar, two-dimensional, incompressible, electrically conducting, and buoyancy-driven convection heat and mass transfer flow form a permeable isothermal sphere embedded in a non-Darcy porosity medium, under the action of an outwardly directed radial magnetic field and Soret (thermodiffusion) and Dufour (diffusion-thermal) effects. Figure 1 illustrates the physical model and coordinate system. Here x is measured along the surface of the sphere, y is measured normal to the surface, respectively, and r is the radial distance from symmetric axis to the surface. in $r = a\sin(x/a)$, a is the radius of the sphere. Both the sphere and the fluid are maintained initially at the same temperature. Instantaneously they are raised to a temperature $T_w(> T_\infty)$ and concentration $C_w(> C_\infty)$ which remain unchanged.

The fluid properties are assumed to be constant except the density variation in the buoyancy force term. The porous medium is simulated using the well-tested and validated non-Darcian drag force model. This incorporates a linear Darcian drag for low velocity effects (bulk impedance of the porous matrix at low Reynolds numbers) and a quadratic (second order) resistance, the Forchheimer drag, for high velocity flows, as may be encountered in chemical engineering systems operating at higher velocities. The appropriate non-Darcian model, following Bég et al. [26, 27], is therefore

$$\nabla p = -\frac{\mu}{K}V - \frac{\rho b}{K}V^2, \tag{1}$$

where ∇p is the pressure drop across the porous medium, μ is the dynamic viscosity of the fluid, b is the Forchheimer (geometric) inertial drag parameter, K is the permeability of the porous medium (hydraulic conductivity), and V is a general velocity. The impressed electrical field is assumed to be zero and both the induced magnetic and electric fields of the flow are negligible in comparison with the applied magnetic field which corresponds to very small magnetic Reynolds number. The Maxwell electromagnetic

field equations, neglecting displacement currents, may be presented, following Sutton and Sherman, thus [28]

$$\begin{aligned} \nabla \cdot \mathbf{B} &= 0 \\ \nabla \times \mathbf{B} &= \mu_0 \mathbf{J} \\ \nabla \times \mathbf{E} &= -\frac{\partial \mathbf{B}}{\partial t} \\ \mathbf{J} &= \sigma[\mathbf{E} + \mathbf{V} \times \mathbf{B}], \end{aligned} \tag{2}$$

where $\mathbf{B}$ is the uniform magnetic field vector, $\mathbf{J}$ is the current density vector, μ_0 is magnetic permeability, σ is the electrical conductivity of the fluid, $\mathbf{E}$ is the electrical field vector, $\mathbf{V}$ is the linear (translational) fluid velocity vector, and t is time. As is customary in engineering magnetohydrodynamics [28], we consider the case for which magnetic lines of force are fixed relative to the fluid. Further, we neglect Hall currents, ionslip currents, and assume steady-state incompressible flow. Since magnetic Reynolds number $\mathrm{Re}_m = \mathrm{Re} = VL/\eta^*$ (based on a general velocity component, V, where η^* is the magnetic diffusivity) is much lower than unity in the present problem, for such scenarios, $\mathrm{Re}_m << 1$, advection is relatively unimportant, and therefore the magnetic field will tend to relax towards a purely diffusive state, determined by the boundary conditions rather than the flow. Magnetic diffusion will be much greater than viscous diffusion and magnetic induction will therefore not arise. The flow regime is also not influenced by the magnetization of the fluid in the applied magnetic field; electrical current is therefore present and the fluid is electrically conducting [28, 29]. In two-dimensional hydromagnetic boundary layer flows, the applied uniform magnetic field vector, $\mathbf{B}$, defined in the Maxwell relations, (2), is assumed to lie in the x-y plane. For steady boundary layer flows, electrical field $\mathbf{E}$ will vanish, as emphasized by Hughes and Young [30]. The Lorentzian hydromagnetic drag will therefore have two components, F_x and F_y, and there will be two components of the applied magnetic field, B_x and B_y. Giving

$$\begin{aligned} F_x &= -\sigma\left(uB_y^2 - vB_xB_y\right) \\ F_y &= \sigma\left(uB_xB_y - vB_x^2\right). \end{aligned} \tag{3}$$

It is customary [28, 30] to assume that B_y varies only with the transverse coordinate, y. For a two-dimensional, steady, uniform applied magnetic field, the Maxwell equation in (1) will reduce to the following, from $\nabla \cdot \mathbf{B} = 0$:

$$\frac{\partial B_x}{\partial x} + \frac{\partial B_y}{\partial y} = 0. \tag{4}$$

Further, assuming

$$\begin{aligned} B_x &= o\left(B_y\right) \\ \frac{\partial}{\partial x} &= o(1) \\ \frac{\partial}{\partial y} &= o(\delta^{-1}), \end{aligned} \tag{5}$$

it follows that the change in B_y across the boundary layer (of thickness δ) will be of the order of δ and may be neglected, so that effectively the hydromagnetic Lorentzian drag force in the x-momentum equation becomes

$$F_x \sim \sigma\, B_y^2(u). \tag{6}$$

In light of the above approximations, and under the usual Boussinesq and boundary layer approximations, the equations for mass continuity, momentum, energy, and concentration can be written as follows:

$$\frac{\partial(ru)}{\partial x} + \frac{\partial(rv)}{\partial y} = 0 \tag{7}$$

$$\begin{aligned} \left(u\frac{\partial u}{\partial x} + v\frac{\partial u}{\partial y}\right) &= \nu\frac{\partial^2 u}{\partial y^2} + g\beta(T - T_\infty)\sin\left(\frac{x}{a}\right) \\ &\quad + g\beta^*(C - C_\infty)\sin\left(\frac{x}{a}\right) - \frac{\sigma B_0^2}{\rho}u \\ &\quad - \frac{\nu}{K}u - \Gamma u^2 \end{aligned} \tag{8}$$

$$u\frac{\partial T}{\partial x} + v\frac{\partial T}{\partial y} = \alpha\frac{\partial^2 T}{\partial y^2} + \frac{D_m K_T}{c_s c_p}\frac{\partial^2 C}{\partial y^2} \tag{9}$$

$$u\frac{\partial C}{\partial x} + v\frac{\partial C}{\partial y} = D_m\frac{\partial^2 C}{\partial y^2} + \frac{D_m K_T}{T_m}\frac{\partial^2 T}{\partial y^2}. \tag{10}$$

The boundary conditions are defined as follows:

$$\begin{aligned} &y = 0: \\ &u = 0, \qquad v = V_w, \qquad T = T_w, \qquad C = C_w, \\ &y \longrightarrow \infty: \\ &u = 0, \qquad T = T_\infty, \qquad C = C_\infty, \end{aligned} \tag{11}$$

where u and v denote the velocity components in the x- and y-directions, respectively, K and B are, respectively, the regime permeability and the Forchheimer inertial drag coefficient of the porous medium, ν is the kinematic viscosity, β and β^* are the coefficients of thermal expansion and concentration expansion, respectively, T and C are the temperature and concentration, respectively, σ is the electrical conductivity, B_0 is the externally imposed radial magnetic field (i.e., applied in the y-direction), ρ is the density, D_m is the mass diffusivity, α is the thermal diffusivity, c_p is the specific heat capacity, c_s is the concentration susceptibility, α is the thermal diffusivity, T_m is the mean fluid temperature, K_T is the thermal diffusion ratio, T_∞ is the free stream temperature, C_∞ is the free stream concentration, and V_w is the uniform blowing/suction velocity at the sphere surface. In the momentum equation (8), the first term on the right hand side simulates the viscous shear, the second is the thermal buoyancy term, the third is the species buoyancy, the fourth is the Lorentzian linear hydromagnetic drag, the fifth term on the right hand side is the porous medium Darcian drag force representing pressure loss due to the presence of the porous medium, and the final term on the

right hand side designates the second-order inertial porous medium drag force (also referred to as the Forchheimer impedance) which accounts for additional pressure drop resulting from interpore mixing appearing at high velocities. The stream function ψ is defined by $ru = \partial(r\psi)/\partial y$ and $rv = -\partial(r\psi)/\partial x$; therefore, the continuity equation is automatically satisfied. Proceeding with the analysis we introduce the following dimensionless variables:

$$\xi = \frac{x}{a}, \qquad \eta = \frac{y}{a}\sqrt[4]{\mathrm{Gr}},$$
$$f(\xi,\eta) = \frac{\psi}{\nu\xi\sqrt[4]{\mathrm{Gr}}}, \qquad \theta(\xi,\eta) = \frac{T-T_\infty}{T_w-T_\infty}, \tag{12}$$
$$\phi(\xi,\eta) = \frac{C-C_\infty}{C_w-C_\infty}, \qquad \mathrm{Gr} = \frac{g\beta(T_w-T_\infty)a^3}{\nu^2}.$$

Substituting (12) into (7)–(11), we obtain

$$f''' + (1+\xi\cot\xi)ff'' - (1+\xi\Lambda)f'^2 + \frac{\sin\xi}{\xi}(\theta+N\phi) - \left(M+\frac{1}{\mathrm{Da}}\right)f' = \xi\left(f'\frac{\partial f'}{\partial\xi} - f''\frac{\partial f}{\partial\xi}\right), \tag{13}$$

$$\frac{\theta''}{\mathrm{Pr}} + (1+\xi\cot\xi)f\,\theta' + \mathrm{Du}\,\phi'' = \xi\left(f'\frac{\partial\theta}{\partial\xi} - \theta'\frac{\partial f}{\partial\xi}\right), \tag{14}$$

$$\frac{\phi''}{\mathrm{Sc}} + (1+\xi\cot\xi)f\,\phi' + \mathrm{Sr}\,\theta'' = \xi\left(f'\frac{\partial\phi}{\partial\xi} - \varphi'\frac{\partial f}{\partial\xi}\right). \tag{15}$$

The transformed dimensionless boundary conditions are

$$\begin{aligned} &\eta = 0: \\ &f' = 0, \qquad f = f_w, \qquad \theta = 1, \qquad \phi = 1, \\ &\eta \longrightarrow \infty: \\ &f' = 0, \qquad \theta = 0, \qquad \phi = 0. \end{aligned} \tag{16}$$

In the above equations, the primes denote the differentiation with respect to η, the dimensionless radial coordinate, f is dimensionless stream function, θ is dimensionless temperature function, ϕ is dimensionless concentration function, $\Lambda = \Gamma a$ is the local inertia coefficient (Forchheimer parameter), $\mathrm{Da} = (K\sqrt{\mathrm{Gr}})/a^2$ is a Darcy parameter, $N = (\beta * (C_w - C_\infty))/(\beta(T_w - T_\infty))$ is the concentration to thermal buoyancy ratio parameter, $\mathrm{Pr} = (\rho\nu c_p)/k$ is the Prandtl number, $\mathrm{Sc} = \nu/D_m$ is the Schmidt number, $M = \sigma B_0^2 a^2/\rho\nu\sqrt{\mathrm{Gr}}$ is the magnetohydrodynamic body force parameter, $\mathrm{Du} = (D_m K_T\,(C_w - C_\infty))/(c_s c_p \nu(T_w - T_\infty))$ is the Dufour number, $\mathrm{Sr} = (D_m K_T(T_w - T_\infty))/(\nu T_m(C_w - C_\infty))$ is the Soret number, $f_w = -V_w a/\nu\sqrt[4]{\mathrm{Gr}}$ is the transpiration (blowing/suction) parameter, and Gr is the Grashof (free convection) parameter. $f_w < 0$ for $V_w > 0$ (the case of injection), and $f_w > 0$ for $V_w < 0$ (the case of suction). The important case of a solid sphere surface is retrieved for $f_w = 0$. The chemical engineering design quantities of physical interest include the skin-friction coefficient, Nusselt number, and Sherwood number, which are given by

$$\frac{C_f}{\rho(\nu/a)^2(\mathrm{Gr})^{3/4}} = \xi f''(\xi,0) \tag{17}$$

$$\frac{\mathrm{Nu}}{\sqrt[4]{\mathrm{Gr}}} = -\theta'(\xi,0) \tag{18}$$

$$\frac{\mathrm{Sh}}{\sqrt[4]{\mathrm{Gr}}} = -\phi'(\xi,0). \tag{19}$$

3. Numerical Method

In this study, the efficient Keller-Box implicit difference method has been employed to solve the general flow model defined by (13) to (15) with boundary conditions (16). This method, originally developed for low speed aerodynamic boundary layers by Keller [31], has been employed in a diverse range of nonlinear magnetohydrodynamics and coupled heat transfer problems. This method is chosen since it seems to be most flexible of the common methods, being easily adaptable for solving equations of any order by Cebeci and Bradshaw [32]. For the sake of brevity, the numerical method is not described. Computations were carried out with $\Delta\xi = 0.1$; the first step size $\Delta\eta = 0.02$. The requirement that the variation of the velocity, temperature, and concentration distribution is less than 10^{-5} between any two successive iterations is employed as the criterion convergence. These include Takhar et al. [33] who studied geothermal hydromagnetic gas convection flow and omitted here for conservation of space. Effectively the complete linearized system is formulated as a block matrix system where each element in the coefficient matrix is a matrix itself. The numerical results are affected by the number of mesh points in both directions. The edge of the boundary-layer y_∞ was adjusted for different ranges of parameters.

4. Results and Discussion

Comprehensive solutions have been obtained and are presented in Figures 2 to 12. The numerical problem comprises **2** independent variables (ξ, η), **3** dependent fluid dynamic variables $(f,\ \theta,\ \phi)$ and 10 thermophysical and body force "control" parameters Pr, M, N, Λ, Da, Sc, f_w, ξ, Sr, and Du. The present code has been extensively validated in numerous problems and benchmarked against shooting quadrature and finite element methods [34–38] and also more recently with Crank-Nicolson difference methods [39–41]. It is extremely reliable and the solutions presented have been rigorously checked. Comparisons are therefore excluded here for conservation of space. In the present computations, the following default parameters are prescribed (unless otherwise stated): $\mathrm{Pr} = 0.71$, $M = 1.0$, $N = 1.0$, $\Lambda = 0.1$, $\xi = 1.0$, $\mathrm{Da} = 0.1$, $\mathrm{Sc} = 0.25$, $f_w = 0.5$ $\mathrm{Du} = 0.2$, and $\mathrm{Sr} = 0.25$. These correspond to weak hydromagnetic convection in electrolytic fluid ($\mathrm{Pr} = 0.71$) flowing through a high permeability ($\mathrm{Da} = 0.1$), high regime with weak blowing ($f_w = 0.5$) at the sphere surface, weak inertial drag ($\Lambda = 0.1$), air diffusing in the electrolytic solution ($\mathrm{Sc} = 0.25$), and

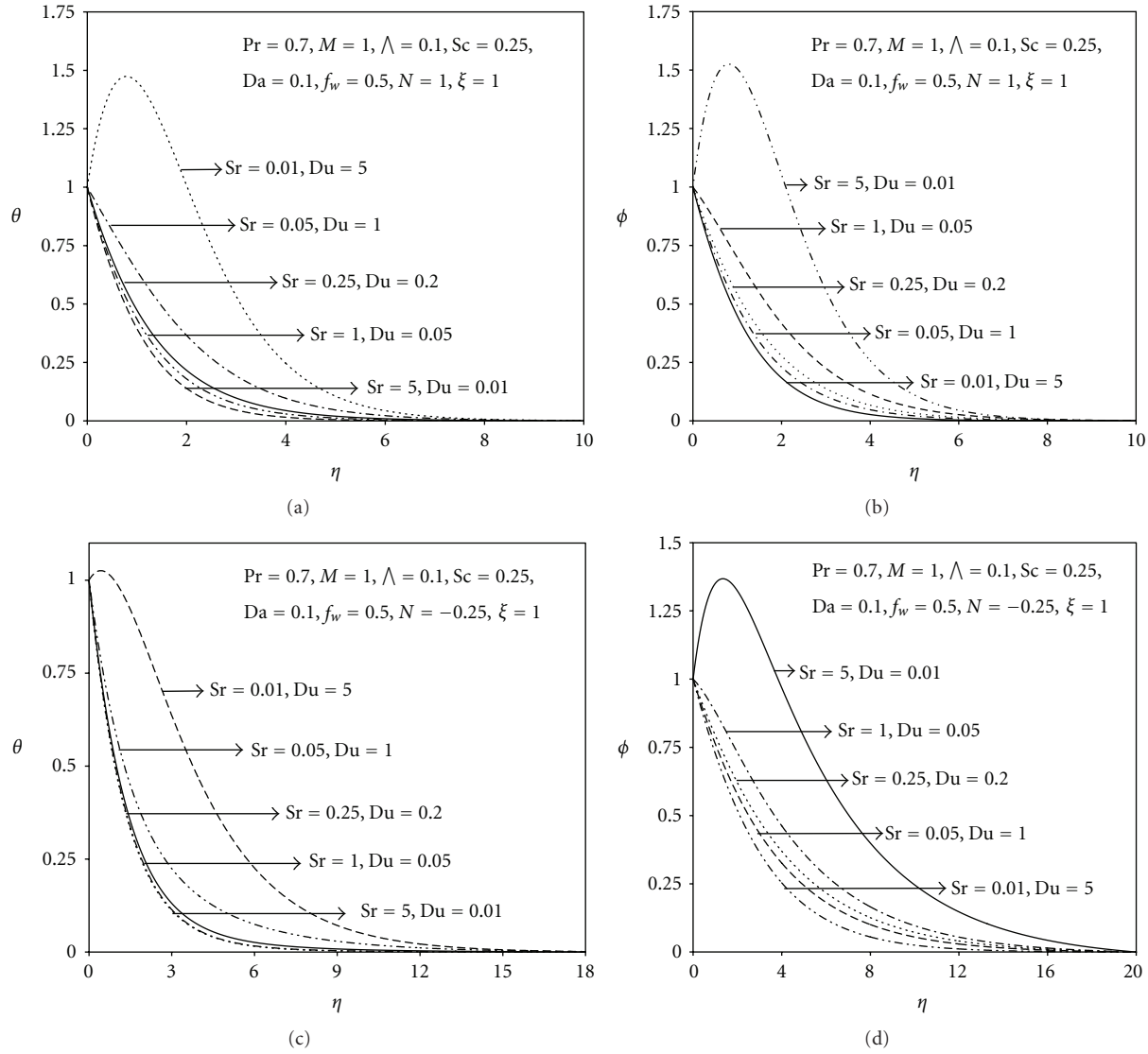

Figure 2: (a) Effect of the Sr and Du on the temperature profiles. (b) Effect of the Sr and Du on the concentration profiles. (c) Effect of the Sr and Du on the temperature profiles with $N = -0.25$. (d) Effect of the Sr and Du on the concentration profiles with $N = -0.25$.

a balance of thermal and species buoyancy forces ($N = 1$), at a general location along the sphere curvature ($\xi = 1$). In addition, we also consider the effect of the streamwise coordinate location on flow dynamics. The value of the parameter ξ is extremely important since in two extreme cases it corresponds to stagnation-point flows. For $\xi \sim 0$, the location is in the vicinity of the lower stagnation point on the sphere. The governing dimensionless equations (13) to (15) in this case reduce to the following ordinary differential equations:

$$f''' + ff'' - f'^2 + (\theta + N\phi) - \left(M + \frac{1}{\mathrm{Da}}\right) f' = 0 \qquad (20)$$

$$\mathrm{Pr}^{-1}\theta'' + f\theta' + \mathrm{Du}\phi'' = 0 \qquad (21)$$

$$\mathrm{Sc}^{-1}\phi'' + f\phi' + \mathrm{Sr}\theta'' = 0. \qquad (22)$$

We note, following Bég et al. [10], the buoyancy term is retained since $(\sin\xi)/\xi \rightarrow 0/0$, that is, 1, so that $(\sin\xi/\xi)(\theta + N\phi) \rightarrow (\theta + N\phi)$; however, the Forchheimer drag force term vanishes at $\xi = 0$, whereas the Darcian drag force and Lorentzian hydromagnetic drag force are retained. The equations however remain strongly coupled. The other extreme case is $\xi \sim \pi$, which physically corresponds to the upper stagnation point on the sphere surface (diametrically opposite to the lower stagnation point).

In Figures 2(a) and 2(b), the influence of Sr and Du on temperature and concentration distributions is illustrated, near the leading edge ($\xi = 0.1$) for the buoyancy-assisted case ($N = 1$). Soret number (Sr) defines the effect of temperature gradients inducing significant mass diffusion effects. Dufour number (Du) measures the contribution of concentration gradients to thermal energy flux in the flow domain. Du and Sr are varied together so that their product

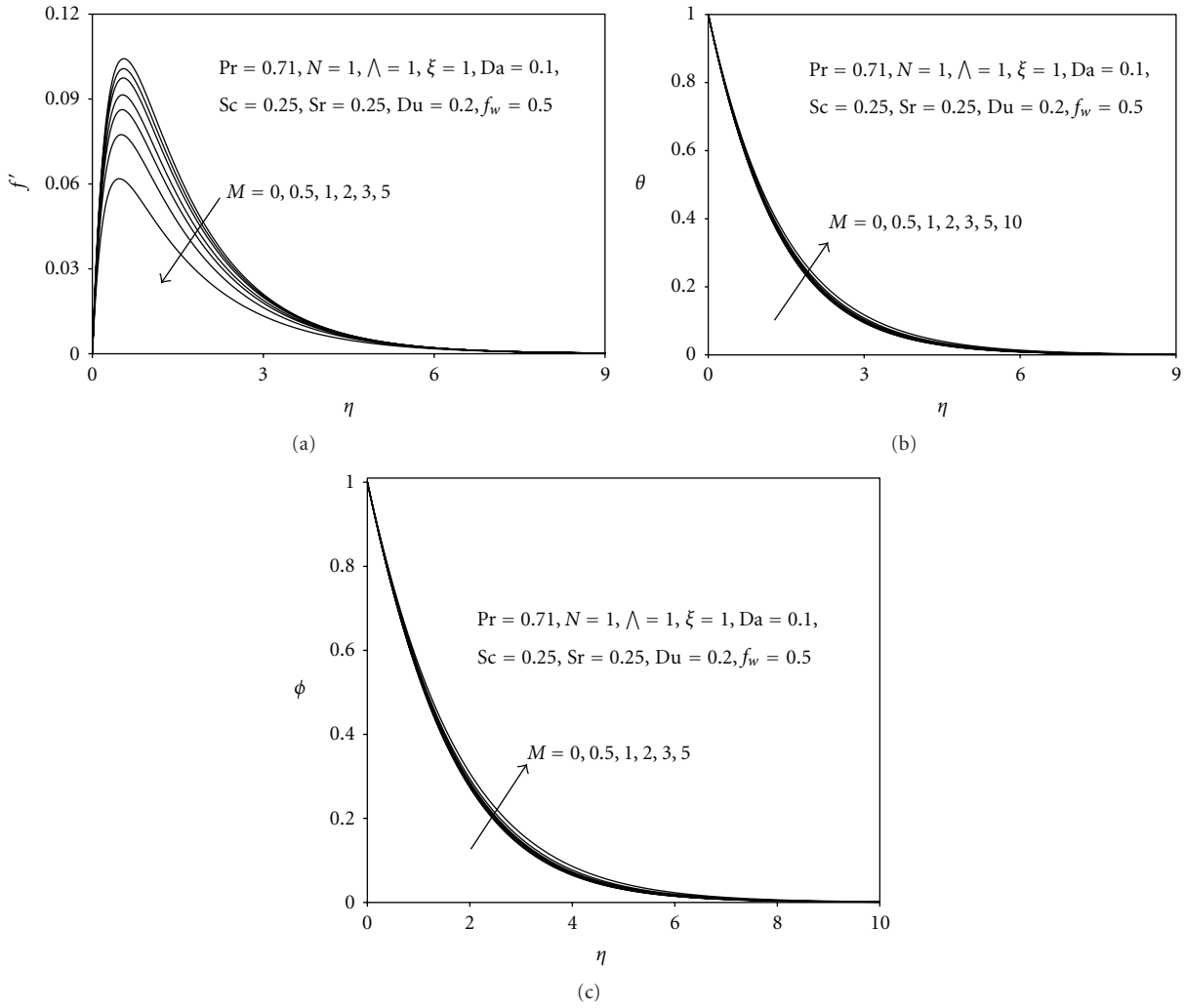

Figure 3: (a) Effect of the M on the velocity profiles. (b) Effect of the M on the temperature profiles. (c) Effect of the M on the concentration profiles.

remains constant: for example, Du = 5.0, Sr = 0.01; Du = 0.01, and Sr = 5.0. An increase in Du (and concurrent decrease in Sr) considerably increases temperature (θ) in the boundary layer, as observed in Figure 2(a). For Du $\leq$ 1, profiles decay smoothly from the wall to zero in the free stream. However, for Du $>$ 1, that is, Du = 5.0, a distinct velocity overshoot exists near the sphere, and thereafter the profile falls to zero at the edge of the boundary layer. Increasing concentration gradients, that is, increasing Du value therefore strongly heats the flow. Increasing Soret number has the exact reverse affect, that is, cooling the boundary layer regime. Figure 2(b) shows that an increase in Soret number due to the contribution of temperature gradients to species diffusion, increases concentration (ϕ) values for all η increasing Du values have the opposite effect. No concentration overshoot is however observed for any values of Soret number which is varied from 0.01 through 0.05, 0.25, and 1.0 to 5.0. The influence of the Soret and Dufour terms will be relatively weak on the velocity fields, and these are therefore not plotted.

For $N > 0$, thermal and concentration buoyancy forces act in unison. For $N = 0$, buoyancy forces are absent, that is, forced convection arises in the regime. For $N < 0$, both buoyancy forces oppose each other. When $N < 0$, we have the case of opposing buoyancy. Particularly, for $N = -0.25$, Figures 2(c) and 2(d), show the temperature and concentration distributions with collective variation in Soret number (Sr) and Dufour number (Du) for the case of buoyancy opposition (opposing buoyancy force, $N <$ 0). Therefore, from the sphere surface, negative N, that is, opposing buoyancy is beneficial to the flow regime, whereas closer to the sphere surface it has a retarding effect. A much more consistent response to a change in the N parameter is observed that temperature throughout the boundary layer is strongly reduced as increase in Sr (and concurrent decrease in Du). We have considered a few cases of larger Sr, Du—this was done to indicate that a concentration overshoot will arise in, for example, Figure 2(d); similarly, with a large Sr = 5.0, we observe that in Figure 2(c) that the temperature distribution deviates noticeably from the profiles for smaller

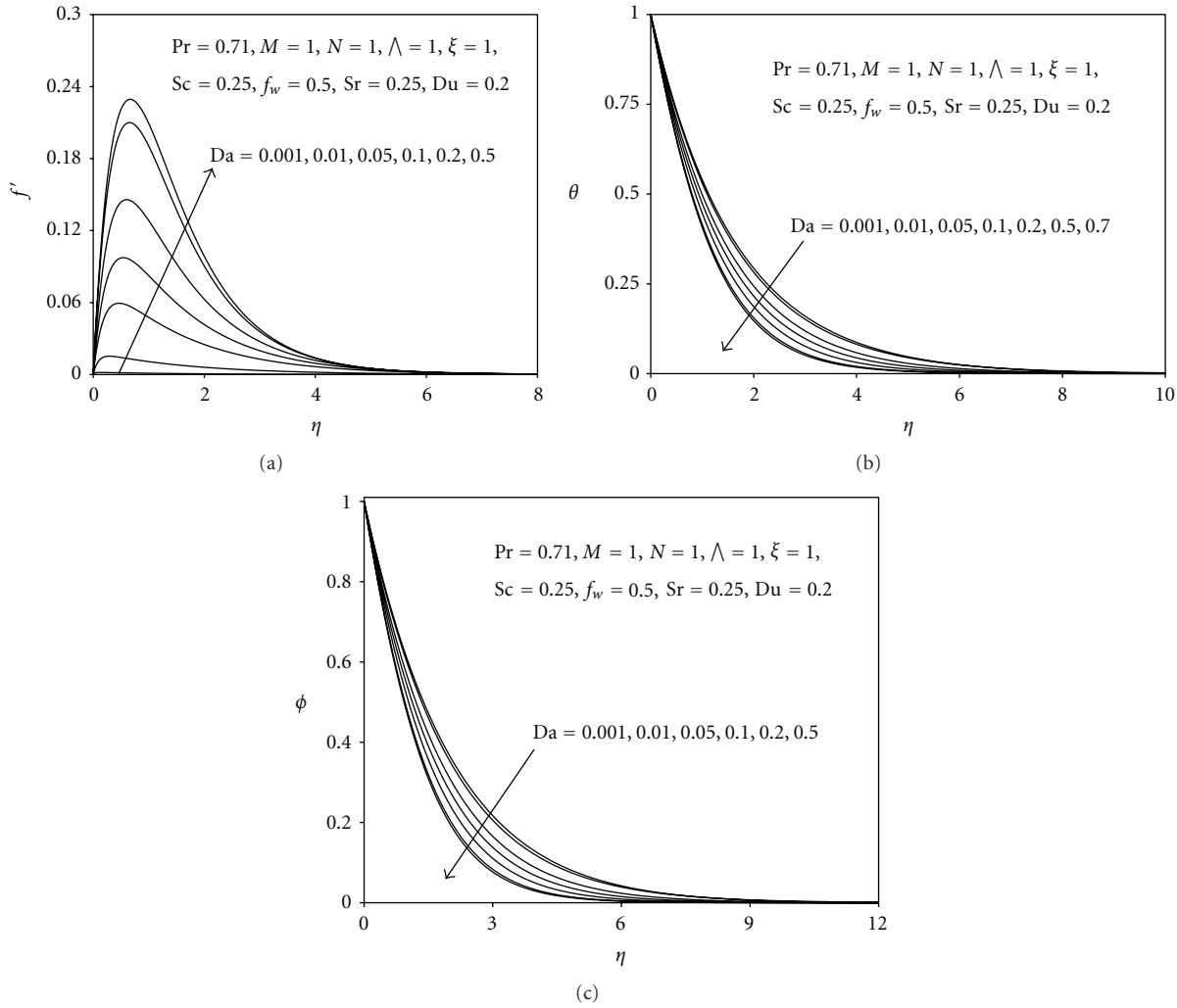

Figure 4: (a) Effect of the Da on the velocity profiles. (b) Effect of the Da on the temperature profiles. (c) Effect of the Da on the concentration profiles.

Sr values. A number of authors have considered the effect of Sr and Du, mainly to address the cases of very strong thermal diffusion encountered in chromatographic applications.

In Figures 3(a) to 3(b) present the response of velocity (f'), temperature (θ), and concentration (ϕ) to magnetohydrodynamic body force parameter (M). $M = \sigma B_0^2 a^2/\rho\nu\sqrt{\mathrm{Gr}}$, and signifies the ratio of Lorentz hydromagnetic body force to viscous hydrodynamic force. Increasing M from 0 (nonconducting case) to 1.0 (magnetic body force and viscous force equal) through to 10.0 (very strong magnetic body force) induces a distinct reduction in velocities as shown in Figure 3(a). With higher M values since the magnetic body force, $-Mf'$ in the momentum equation (13) is amplified; this serves to increasingly retard the flow. The imposition of a radial magnetic field is therefore a powerful mechanism for inhibiting flow in the regime. The maximum velocities as before arise close to the sphere surface, a short distance from it (at the sphere surface, $\eta = 0$, and velocity vanishes in consistency with the no-slip condition, that is, $f' = 0$); with further distance into the boundary layer, the profiles converge, that is, the magnetic body force has a weaker effect in the far field regime than in the near-field regime. Conversely with increasing M, temperature, (Figure 3(b)) is observed to be markedly increased. This is physically explained by the fact that the extra work expended in dragging the fluid against the magnetic field is dissipated as thermal energy in the boundary layer, as elucidated by Sutton and Sherman [28], Pai [29], and Hughes and Young [30]. This results in heating of the boundary layer and an ascent in temperatures, an effect which is maximized some distance away from the sphere surface. The magnetic field influence on temperatures while noticeable is considerably less dramatic than that on the velocity field, since the Lorentz body force only arises in the momentum equation (13) and influences the temperature (θ) and concentration (ϕ) fields, only via the thermal and buoyancy terms, $(\sin\xi/\xi)(\theta + N\phi)$. Magnetic effects do not feature in either the temperature (14) or species diffusion equations (15). The deceleration in flow serves to enhance species diffusion in the regime and this causes a rise also in the concentration profiles

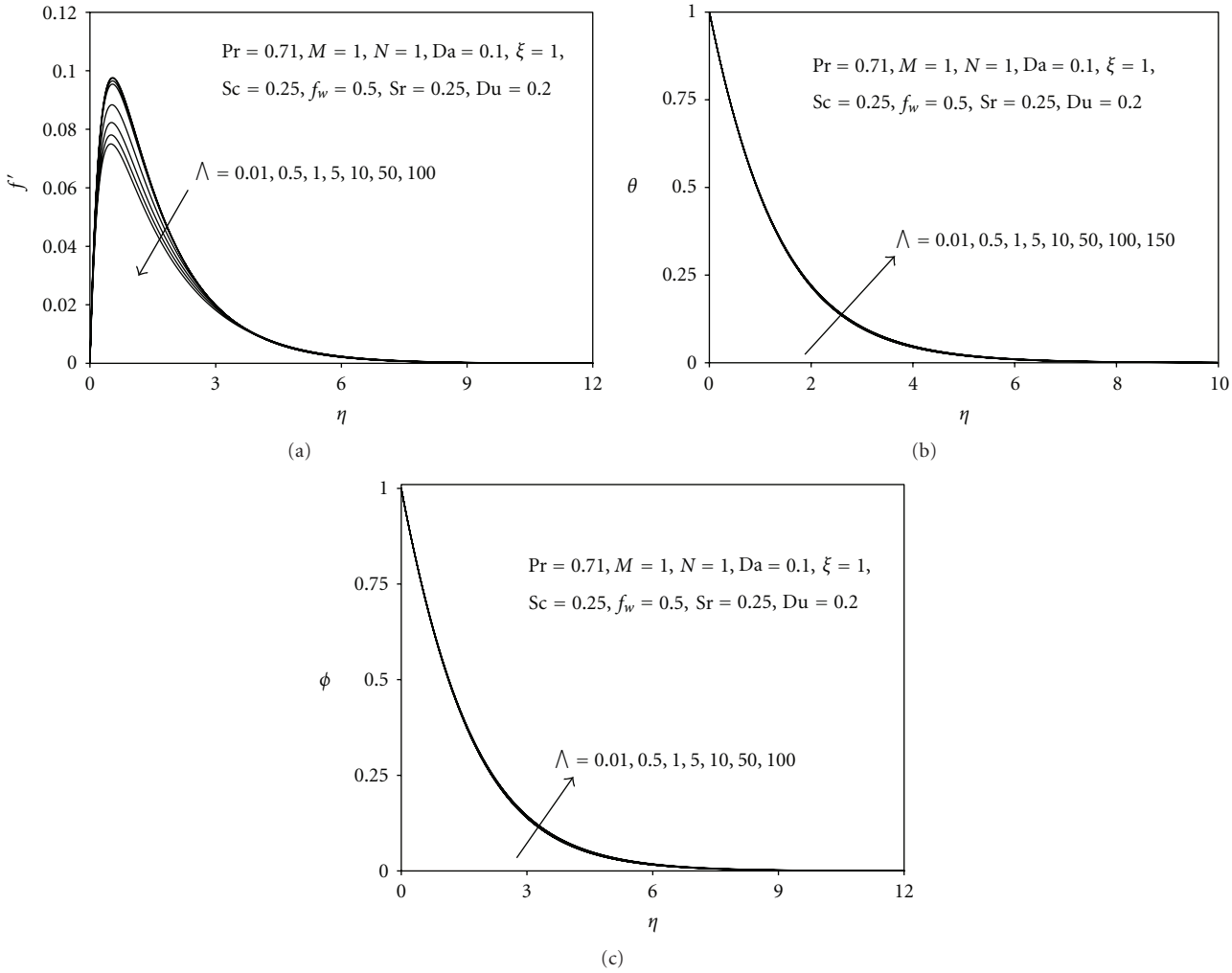

Figure 5: (a) Effect of the Λ on the velocity profiles. (b) Effect of the Λ on the temperature profiles. (c) Effect of the Λ on the concentration profiles.

(Figure 3(c)) with increasing magnetic parameter. Applied radial magnetic field, therefore, while counteracting the momentum development in the regime, serves to enhance the heat and species diffusion, and this is of immense benefit in chemical engineering operations, where designers may wish to elevate transport in a regime without accelerating the flow.

In Figures 4(a) to 4(c), the variation of velocity (f'), temperature (θ), and species concentration (ϕ) with transverse coordinate (η) over a wide range of Darcy parameters is illustrated. The Darcian body force, $(1/\mathrm{Da})f'$ features only in the momentum equation (13). This body force although linear is inversely proportional to the Darcy parameter, $Da = (K\sqrt{\mathrm{Gr}})/a^2$ which itself is a measure of the permeability of the regime, that is, hydraulic transmissivity of the porous medium to fluid percolation. Increasing Da from 0.001 (extremely low permeability) through 0.01, 0.05, 0.1, 0.15 to the maximum value of 0.2, clearly substantially enhances the flow velocity in the boundary layer. With higher Da values, there will be a corresponding reduction in the Darcian drag force, and this will serve to effectively accelerate the flow in the medium adjacent to the sphere. In all the velocity profiles, the peak velocity is located close to the sphere surface; with an increase in Da, this peak is displaced progressively away from the sphere surface. Temperature (θ), however, as shown in Figure 4(b), is observed to progressively decrease with an increase in Darcy number (Da). With increasing Da, there is a decrease in the density of solid matrix fibers in the regime (permeability is increased). As such, thermal conduction is depressed and this reduces the temperatures in the boundary layer. The greatest reduction in temperatures arises at some distance form the sphere surface. In all cases, the profiles decay smoothly to zero in the free stream. The quality of the Keller-box mesh is emphasized by the smooth asymptotic tendency of the profiles far from the wall. The specification of an adequate distance for infinity boundary conditions is therefore confirmed. Concentration profiles (ϕ) are depressed even more strongly than temperature profiles, with an increase in Darcy number, as shown in Figure 4(c). With N set to unity, both thermal and species buoyancy

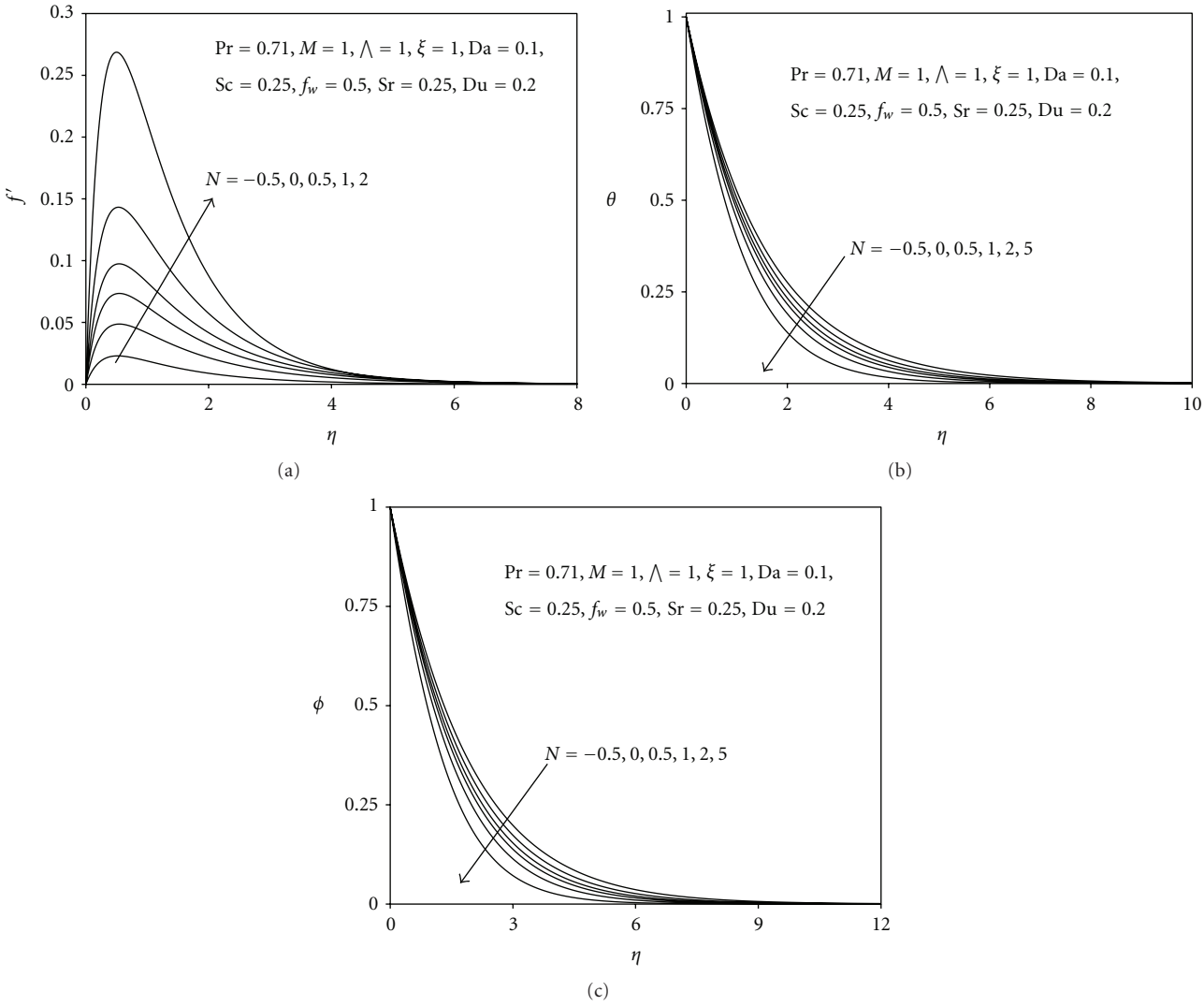

Figure 6: (a) Effect of the N on the velocity profiles. (b) Effect of the N on the temperature profiles. (c) Effect of the N on the concentration profiles.

forces in the momentum equation have the same magnitude. With lesser fibers in the regime, the diffusion of species would be expected to be enhanced. However, it has been documented by numerous experimental studies that lower permeability regimes in fact enhance species diffusion, as opposed to counteracting it. Our results are in excellent agreement with the findings of Vafai and Tien [42].

Figures 5(a) to 5(c) show the influence of the Forchheimer inertial parameter (Λ) on the flow variables. This parameter is associated with the second-order Forchheimer resistance term, $\xi\Lambda(f')^2$, in (13). Forchheimer drag is directly proportional to the parameter, Λ. An increase in Λ evidently strongly retards the flow, as illustrated in Figure 5(a), for some considerable distance into the in boundary layer, transverse to the sphere surface. Beyond a certain point however negligible effects are observed. Bear [43] has highlighted that Forchheimer effects are associated with higher velocities in porous media transport. Forchheimer drag however is quadratic and the increase in this "form" drag swamps the momentum development, effectively decelerating the flow. We note that the deviation from the linear, the nonlinear behavior in porous media is gradual unlike the sharp change from laminar to turbulence flow in the case of fluid flow in conduits. As such, there are no sudden changes in velocity profile with increasing Forchheimer parameter, that is, no fluctuations in the velocity field. This confirms the modern perspective of many researchers [44, 45] that the main cause of deviation from the Darcian behavior is related to other factors different than those which contribute to turbulence. The drag force model employed in this study is physically logical since it implies that non-Darcy flow is occurring at high spatial velocity in porous media as a consequence of geometrical factors rather than attributing this behavior to "turbulence" phenomena. In this context, the term "non-Darcian" does not allude to a different regime of flow, but to the amplified effects of Forchheimer drag at

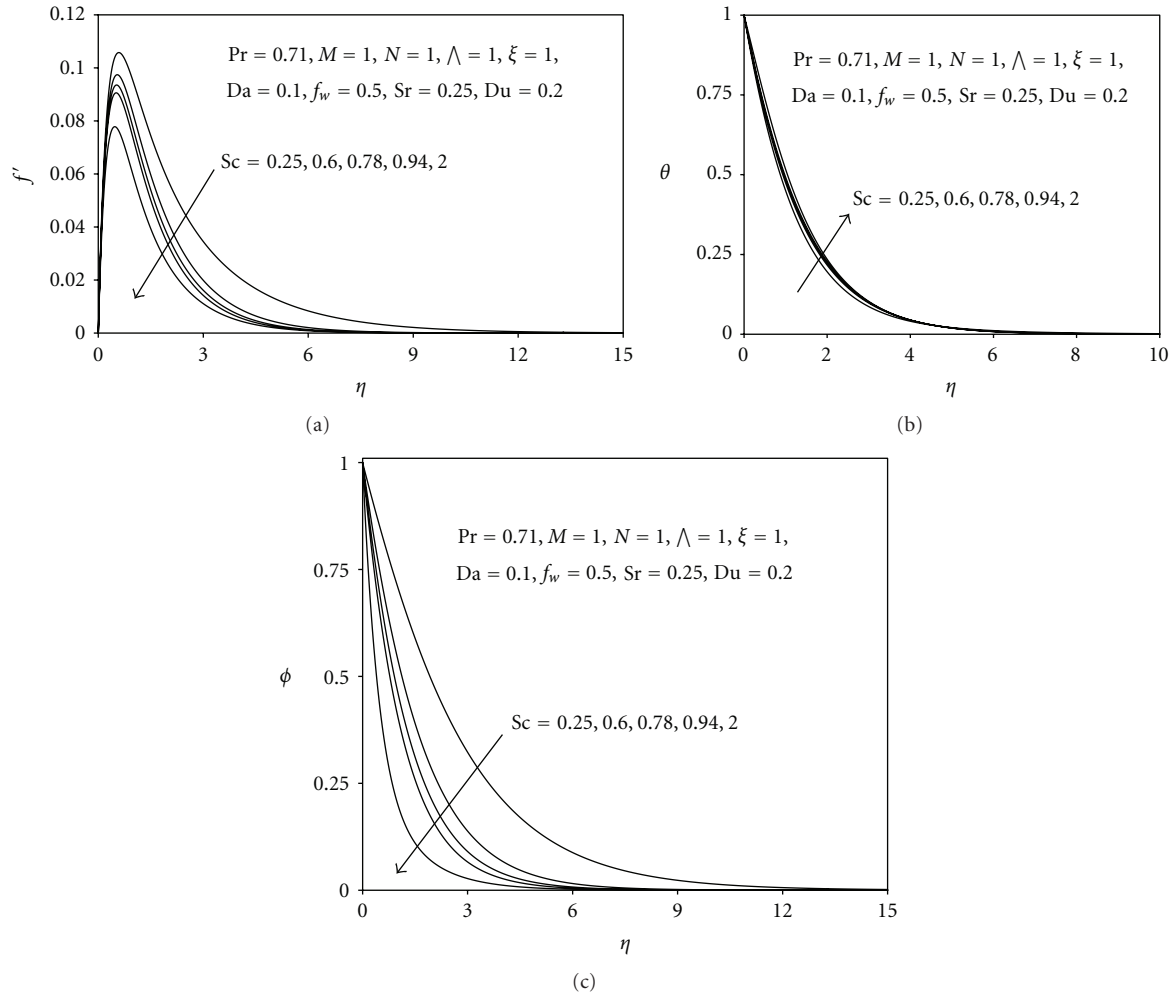

Figure 7: (a) Effect of the Sc on the velocity profiles. (b) Effect of the Sc on the temperature profiles. (c) Effect of the Sc on the concentration profiles.

higher velocities, as elaborated by a number of other studies [46]. With a dramatic increase in Λ, there is a very slight elevation in temperatures (Figure 5(b)) in the regime. The deceleration in the flow results in thinner velocity boundary layers which serve to enhance energy diffusion. The influence on the concentration (species diffusion) field (Figure 5(c)) is similar to that of the temperature field but more pronounced. Species concentration (ϕ) is slightly increased, especially at some distance from the sphere surface, with an increase in Forchheimer parameter, Λ.

Figures 6(a) to 6(c) depict the effect of the buoyancy ratio parameter (N) on the velocity, temperature, and species concentration variables. $N = (\beta * (C_w - C_\infty))/(\beta(T_w - T_\infty))$ is a key parameter controlling the transport phenomena in the regime. For $N > 0$ thermal and concentration buoyancy forces act in unison. For $N = 0$, buoyancy forces are absent, that is, forced convection arises in the regime. For $N < 0$, both buoyancy forces oppose each other. Inspection of Figure 6(a) indicates that for $N > 0$, that is, aiding buoyancy forces, the flow velocities are greatly enhance. Positive N therefore as expected accelerates the flow. With an increase in N, the velocity peaks progressively migrate further from the sphere surface. Figures 6(b) and 6(c) reveal that temperature, θ, and concentration, ϕ, exhibit the converse response to a positive increase in buoyancy ratio, N; both are considerably reduced. Although the buoyancy parameter does not arise in either the thermal boundary layer (heat conservation) (14) or the concentration boundary layer (species diffusion conservation) (15), via coupling with the term, $(\sin \xi/\xi)(\theta + N\phi)$ in the momentum equation (13), N exerts a strong influence on both energy and species diffusion in the boundary layer. For all values of N there is a smooth decay in both θ and ϕ profiles from a maximum at the sphere surface to the free stream. The buoyancy effect can clearly be exploited to control effectively both temperature and concentration distributions in such a regime, and this again is of considerable utility to chemical engineering designers involved in packed bed transport phenomena systems. We further note that since N is directly coupled with the species field in the buoyancy term, it will exert a more pronounced effect on the concentration distributions than on the temperature profiles. This explains the greater

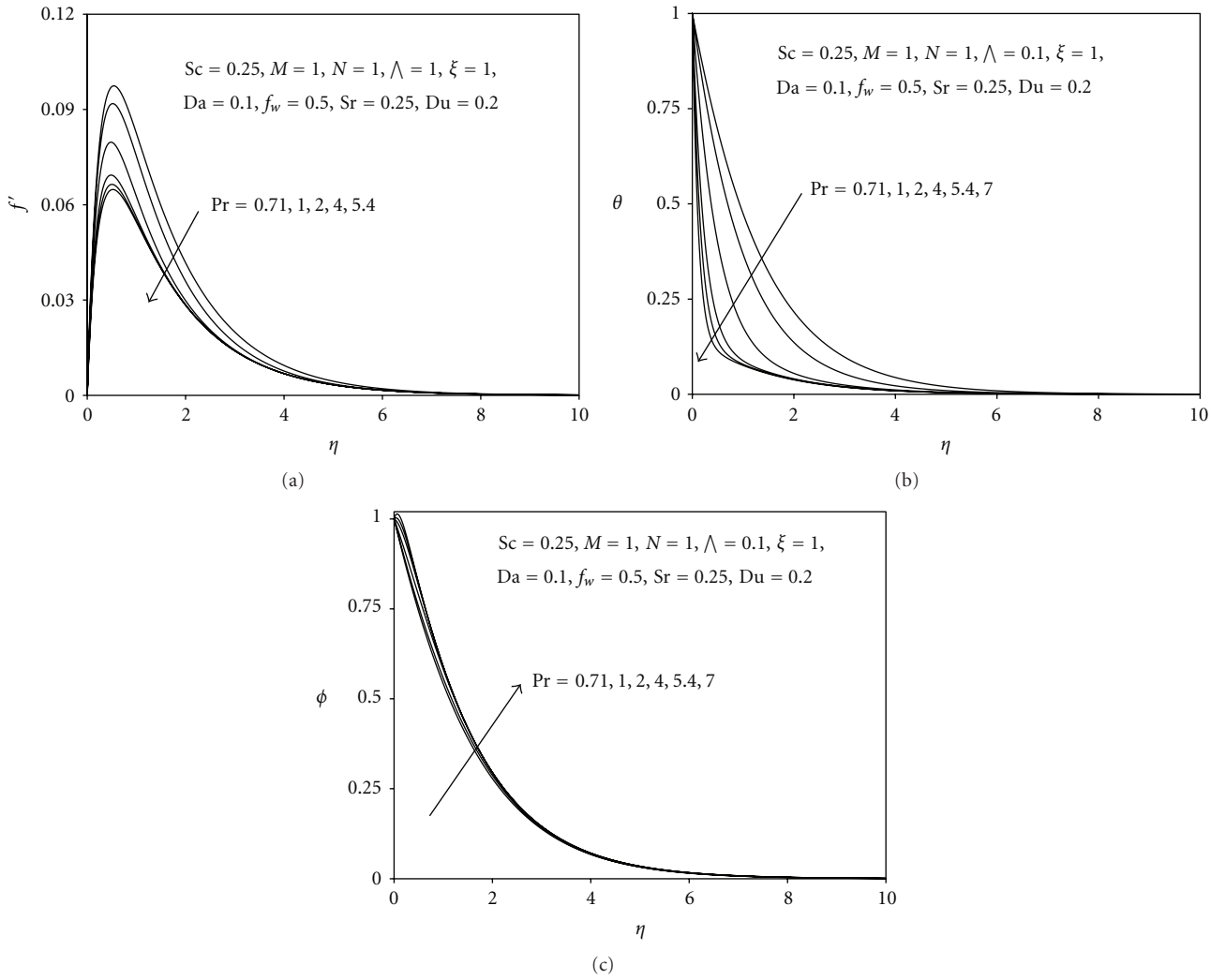

Figure 8: (a) Effect of the Pr on the velocity profiles. (b) Effect of the Pr on the temperature profiles. (c) Effect of the Pr on the concentration profiles.

decreases in concentration values (Figure 6(c)) over the same range of N increase (from 0 through 0.1, 0.5, 1.0 to 2.0), compared with the reduction in the temperature profiles (Figure 6(b)).

Figures 7(a) to 7(c) illustrate the influence of Schmidt number (Sc) on velocity (f'), temperature (θ), and species concentration (ϕ). Velocity (Figure 7(a)) is strongly reduced with an increase in Sc from 0.25 through 0.6, 0.78, and 0.94 to 2.0. Sc represents the ratio of the mass (species) and viscous diffusion time sales. It is also the ratio of momentum diffusivity to species diffusivity. For Sc < 1, the momentum diffusivity is lower than the species (mass) diffusivity and the species diffusion rate exceeds the momentum diffusion rate. For Sc > 1, this scenario is reversed. Higher values of Sc correspond to higher density species diffusing in air for example, Sc = 1.0 corresponds to methanol diffusing in electrically conducting air, Sc = 2.0 implies ethylbenzene diffusing in air. Increasing Sc lowers the chemical molecular diffusivity of the species. As Sc is increased, the concentration boundary layer will become relatively thinner than the viscous (momentum) boundary layer. Velocity will therefore be reduced. For the special case of Sc = 1.0, the velocity and concentration boundary layers will be of the same thickness and both momentum and species will be diffused at the same rate. Inspection of Figure 7(b) shows that temperatures (θ) are enhanced with an increase in Sc; however, the alteration in profiles is not dramatic. In Figure 7(c), the concentration profiles are, as expected, found to be much more markedly affected by a rise in Sc values. ϕ values are strongly reduced with increasing Sc values. With thinner concentration boundary layers, the concentration gradients will be enhanced causing a decrease in concentration of species in the boundary layer. For Sc < 1, species diffusivity exceeds momentum diffusivity and this accounts for the greater concentration values for Sc = 0.25, 0.6, 0.78, 0.94 compared with the minimized concentration profile for Sc = 2.0, since in this latter case Sc > 1, that is, momentum diffusivity exceeds mass (species) diffusivity. The implication

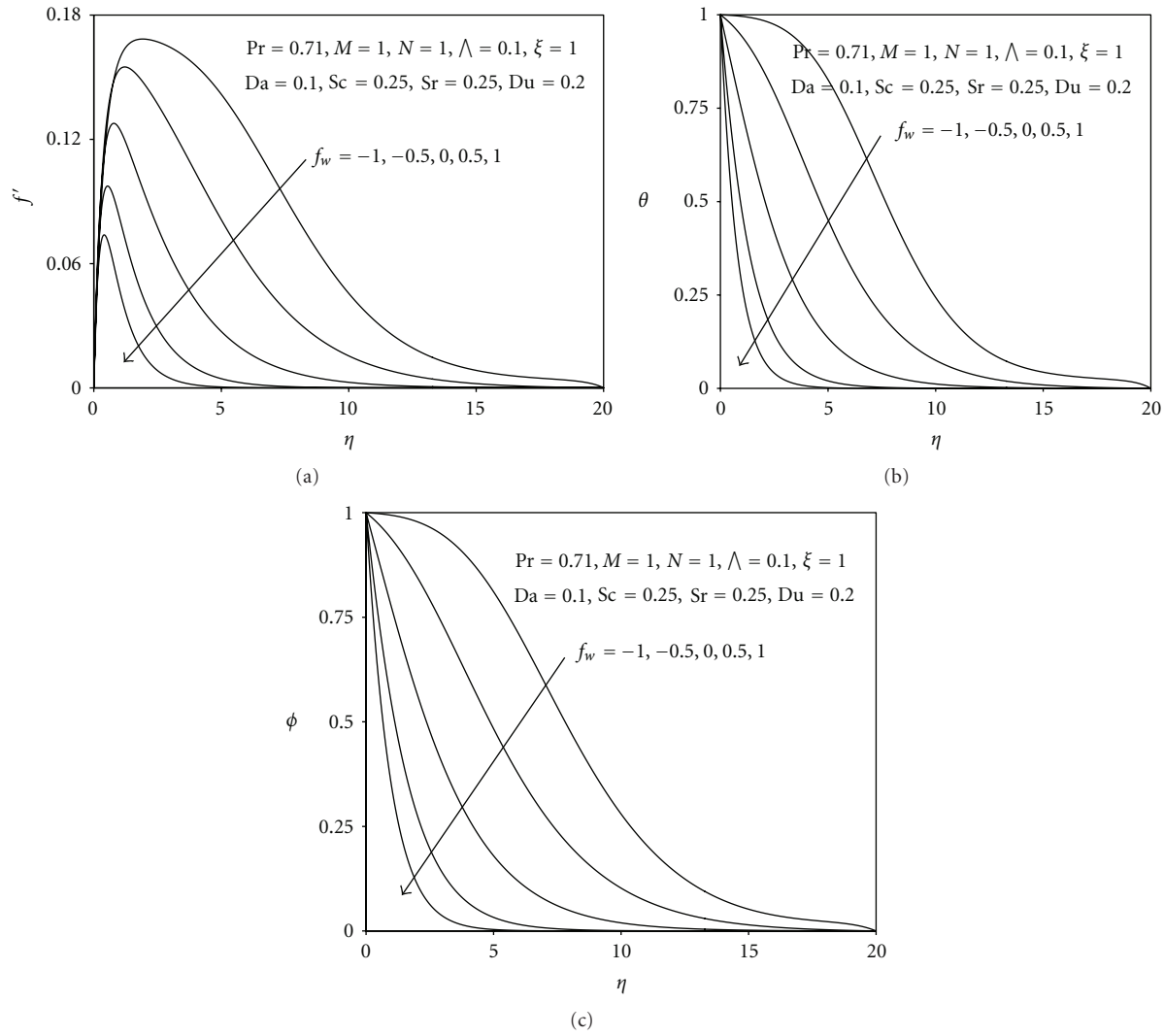

FIGURE 9: (a) Effect of the f_w on the velocity profiles. (b) Effect of the f_w on the temperature profiles. (c) Effect of the f_w on the concentration profiles.

for chemical engineering designers is that in such a regime, a lower Schmidt number diffusing species must be employed to enhance concentration distributions in the medium.

Figures 8(a) to 8(c) present the effect of Prandtl number (Pr) on the primitive flow variables of velocity, temperature, and concentration. Prandtl number signifies the ratio of viscous diffusion to thermal diffusion in the boundary layer regime. With greater Pr values, viscous diffusion rate exceeds thermal diffusion rate. An increase in Pr from 0.71 (air) through 1.0, 2.0, 4.0, 5.4 to 7.0 (conducting water e.g., saline solution) strongly depresses velocities (Figure 8(a)) in the regime. For Pr < 1, thermal diffusivity exceeds momentum diffusivity, that is, heat will diffuse faster than momentum. For Pr = 1.0, both the viscous and energy diffusion rates will be the same as will the thermal and velocity boundary layer thicknesses. For Pr > 1, momentum diffusivity will exceed thermal diffusivity. As such for lower Pr fluids, velocities we expect to be maximized and this is indeed testified to by Figure 8(a). Higher Pr fluids will correspond to lower velocities. Similarly temperatures (θ), as shown in Figure 8(b), are also considerably lowered with an increase in Pr. Prandtl number also represents the product of dynamic viscosity and specific heat capacity divided by thermal conductivity of the primary fluid ($\Pr = (\rho \nu c_p)/k \equiv (\mu c_p)/k$). Higher Pr fluids (e.g., Pr = 7.0 for electrically conducting water) will therefore possess a much lower thermal conductivity and this will result in a significant decrease in temperatures in the boundary layer. Conversely lower Pr fluids will possess a much greater thermal conductivity (e.g., Pr = 0.7 for conducting air) and will generate much higher temperatures. All temperatures are observed to decay smoothly from a maximum at the wall to zero in the free stream of the boundary layer. In Figure 8(c), the concentration profiles are seen to be enhanced in magnitude with increasing Pr values. Prandtl number is a thermophysical property at a given temperature and pressure. As such, it is associated with actual liquids. It will exert a similar influence on the temperature distribution whether in the pure free convection or pure forced convection scenarios. This is disadvantageous to the temperature field but beneficial to the species diffusion

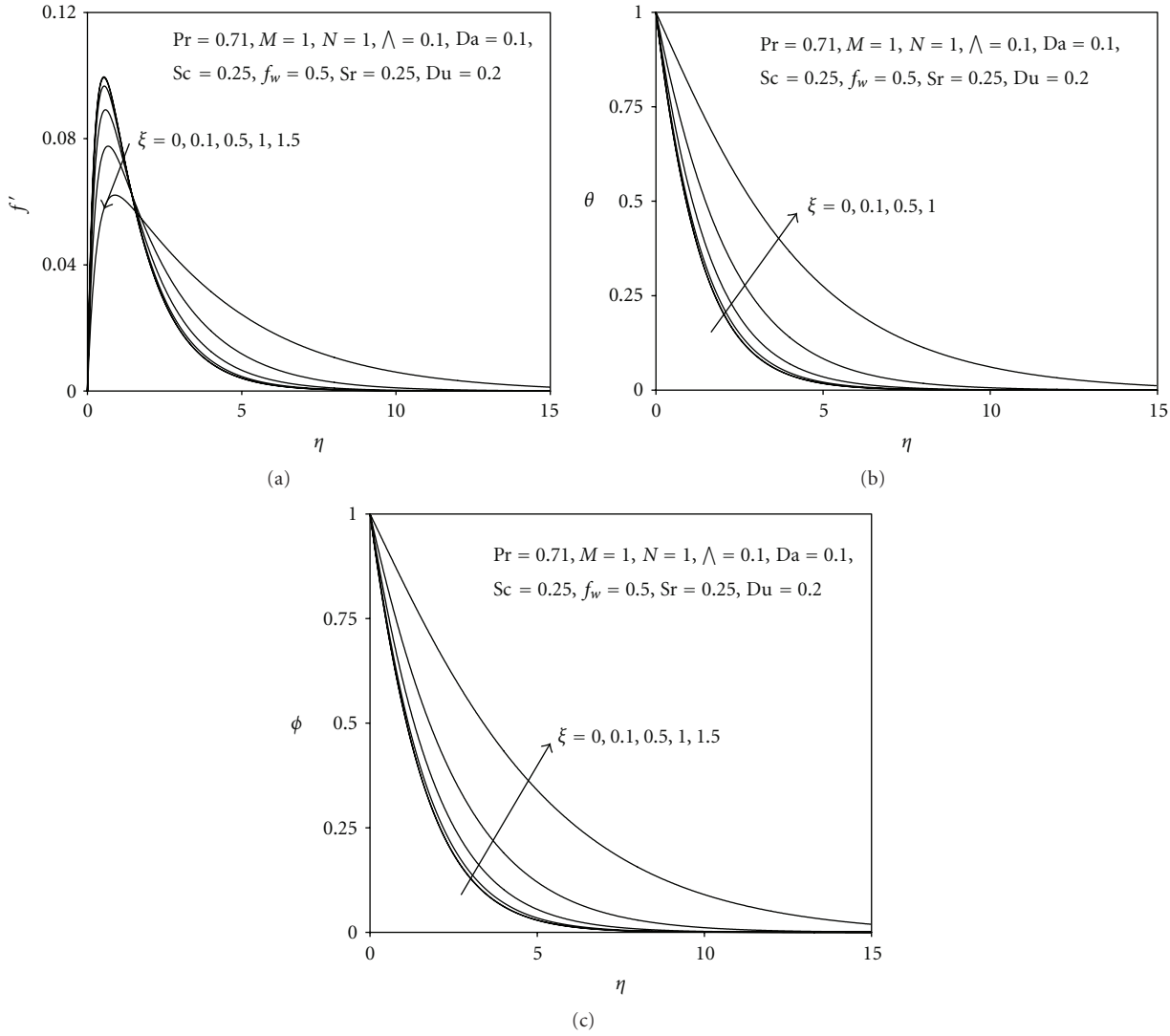

Figure 10: (a) The velocity profiles with various values of ξ. (b) The temperature profiles with various values of ξ. (c) The concentration profiles with various values of ξ.

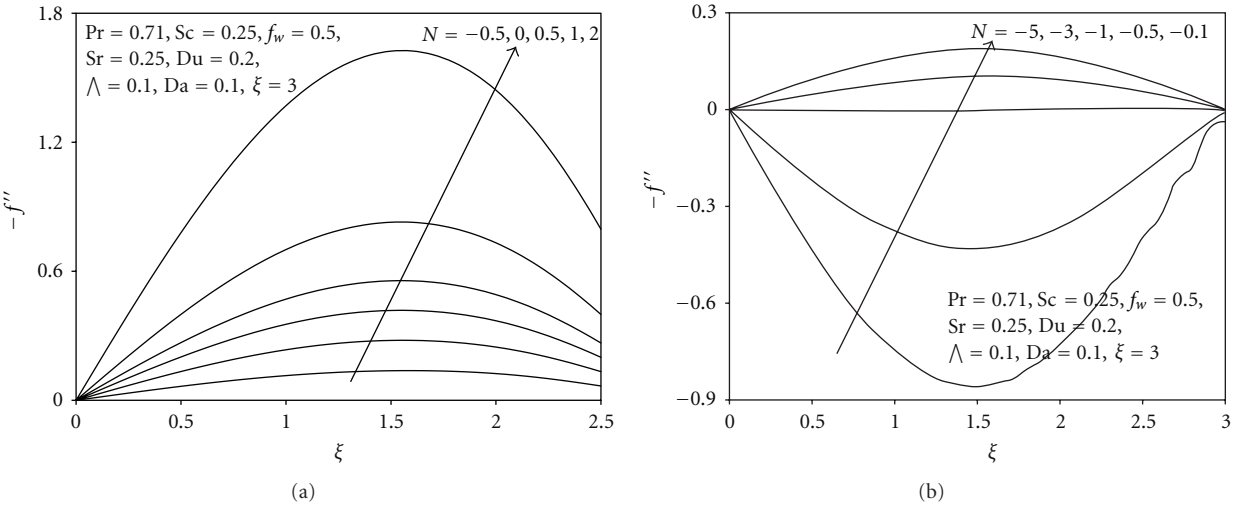

Figure 11: (a) Skin friction coefficient results for various values of N. (b) Skin friction coefficient results for negative values of N.

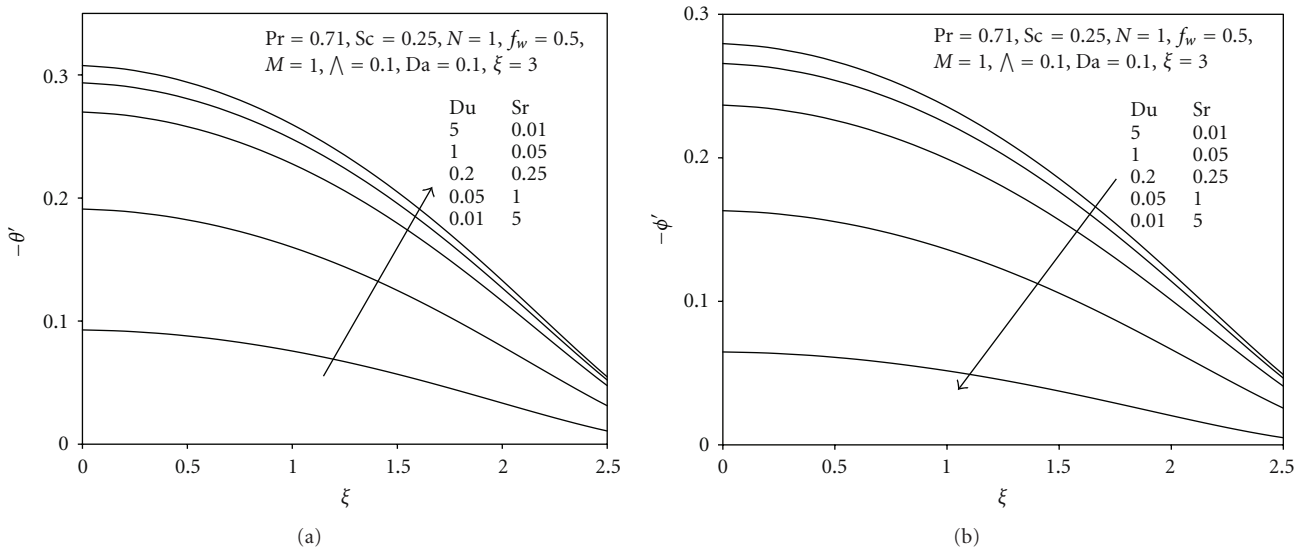

Figure 12: (a) Local Nusselt number results for various values of Sr and Du. (b) Local Sherwood number results for various values of Sr and Du.

field since greater momentum diffusion aids the advection of mass in the flow. In chemical engineering design applications (e.g., chromatographical transport phenomena), therefore to achieve a better distribution of species across the boundary layer (transverse to the sphere surface), higher Prandtl number liquids will be more logical than lower Prandtl numbers. The interplay of momentum, thermal, and species diffusion will imply inevitably that all three variables cannot be simultaneously maximized, irrespective of the magnitude of the buoyancy forces involved. A strategic approach is therefore required in selecting primary fluids which posses high thermal diffusivities (low Prandtl numbers) for temperature enhancement or low thermal diffusivities (high Prandtl numbers) for species diffusion enhancement. Such aspects would clearly require more rigorous experimental observations to which the present theoretical and numerical study is complimentary.

Figures 9(a) to 9(c) depict the distributions of velocity, temperature and concentration with wall transpiration parameter (f_w). We have restricted attention here only to the case of suction (lateral mass withdrawal through the sphere surface out of boundary layer regime). With an increase in suction ($f_w > 0$), the velocity is clearly decreased, that is, flow decelerated. Velocity is therefore maximized for the solid sphere case ($f_w = 0$). Increasing suction causes the boundary layer to adhere closer to the flow and destroys momentum transfer; it is therefore an excellent control mechanism and has been exploited in numerous technologies including aerodynamics where flow control is imperative [47]. Temperature, θ, and concentration, ϕ, as depicted in Figures 9(b) and 9(c), respectively, are also markedly stifled with increased suction at the sphere wall and depressed with increased suction. The temperature and concentration profiles, once again assume a continuous decay from the wall to the free stream, whereas the velocity field (Figure 9(a)) initially ascends, peaks, and then decays into the free stream. The strong influence of wall transpiration on all the flow variables is clearly identified and again such a mechanism (as with magnetic field, porous media drag forces and buoyancy forces) discussed earlier is greatly beneficial in allowing flow control and regulation of heat and mass transfer characteristics in such regimes.

Figures 10(a) to 10(b) depict the velocity, temperature, and species concentration distributions transverse to the sphere wall for various streamwise coordinate values, ξ. Velocity is clearly decelerated with increasing migration from the leading edge, that is, larger ξ values (Figure 10(a)) for some distance into the boundary layer, transverse to the wall ($\eta \sim 20$). However, closer to the free stream, this effect is reversed and the flow is accelerated with increasing distance along the sphere surface. Conversely a very strong increase in temperature (θ) and concentration (ϕ), as shown in Figures 10(b) and 10(c), occurs with increasing ξ values. Also unlike the velocity response which ascends from the surface of the spheres, and peaks and then decreases further into the boundary layer (Figure 10(a)), the temperature and concentration fields both decrease continuously across the boundary layer transverse to the wall. Temperature and concentration are both minimized at the leading edge and maximized with the greatest distances along the sphere surface from the leading edge.

The influence of buoyancy ratio, N, on skin friction, that is, local shear stress at the sphere surface is presented in Figures 11(a) and 11(b) for negative and positive, respectively. Positive N values clearly accentuate $-f''$ values, whereas negative N values cause a depression in skin friction. As elucidated earlier, aiding buoyancy forces ($N > 0$) serve to accelerate the flow and this will increase skin friction at the

sphere wall; opposing thermal and species buoyancy forces will exert the opposite effect and cause a flow deceleration leading to a decay in skin friction magnitudes.

Figure 12(a) shows the variation of local Nusselt number, $-\theta'(\xi, 0)$ with the combined effects of Soret and Dufour number. Increasing Soret number (Sr) and simultaneously reducing Dufour (Du) number greatly boosts the local heat transfer rate at the sphere surface. With increasing distance from the leading edge ($\xi = 0$), however, the profiles all decrease.

Figure 12(b) presents the local Sherwood number distribution with streamwise coordinate, ξ, for various Soret and Dufour numbers. Increasing Dufour number and decreasing Soret number strongly enhance the mass transfer rate at the wall, that is, boosts $-\phi'(\xi, 0)$ values. Generally with greater distance along the sphere surface, that is, with increasing ξ values, the local Sherwood number decreases. However, for very low Dufour numbers (Du = 0.05, 0.01) and very high Soret numbers (Sr =1.0 and 5.0, resp.) there is a slight upturn in $-\phi'(\xi, 0)$ at large distances from the leading edge. The species cross-diffusion term, Du ϕ'', in the energy equation (14) and the temperature cross-diffusion term, Sr θ'', in the species equation (15) clearly exert a significant influence on both heat transfer and mass transfer rates at the sphere surface in the porous media regime and should not be ignored in advanced studies of importance in materials processing.

5. Conclusions

A detailed mathematical study of the steady, laminar, incompressible hydromagnetic buoyancy-driven convective boundary layer heat and mass transfer from a spherical body immersed in a saturated non-Darcy porous medium with Soret/Dufour effects has been conducted. Numerical solutions have been obtained for the normalized conservations equations. It has been shown that increasing magnetic field generally decelerates the flow but increases temperatures and concentration values in the regime. Increasing porosity serves to accelerate the flow but reduce temperatures and concentration values. Increasing Forchheimer (second order) porous form drag tends to strongly retard the flow but enhance temperatures and concentration values. The present numerical code based on the robust, implicit Keller-box finite difference method has been shown to produce excellent results. Very good correlation between the present computations and the trends of other previous studies has been identified. Further investigations will consider transient effects and also employ the Keller-box method to consider more complex chemical engineering phenomena including electrophoretic deposition, nanofluids, and thermophoresis.

Acknowledgment

The authors are grateful to both reviewers for their constructive comments which have helped to improve the present paper.

References

[1] S. Yesilyurt, L. Vujisic, S. Motakef, F. R. Szofran, and M. P. Volz, "Numerical investigation of the effect of thermoelectromagnetic convection (TEMC) on the Bridgman growth of Ge1-xSix," *Journal of Crystal Growth*, vol. 207, no. 4, pp. 278–291, 1999.

[2] J. C. T. Eijkel, C. Dalton, C. J. Hayden, J. P. H. Burt, and A. Manz, "A circular ac magnetohydrodynamic micropump for chromatographic applications," *Sensors and Actuators, B*, vol. 92, no. 1-2, pp. 215–221, 2003.

[3] I. Iliuta and F. Larachi, "Magnetohydrodynamics of trickle bed reactors: mechanistic model, experimental validation and simulations," *Chemical Engineering Science*, vol. 58, no. 2, pp. 297–307, 2003.

[4] T. L. Sanders, *Magnetohydraulic flow through a packed bed of electrically conducting spheres [Ph.D. thesis]*, University of Texas at Austin, Austin, Tex, USA, 1985.

[5] T.-B. Chang, O. Anwar Bég, and E. Kahya, "Numerical study of laminar incompressible velocity and magnetic boundary layers along a flat plate with wall effects," *International Journal of Applied Mathematics and Mechanics (IJAMM)*, vol. 6, pp. 99–118, 2010.

[6] S. Rawat, R. Bhargava, R. Bhargava, and O. Anwar Bég, "Transient magneto-micropolar free convection heat and mass transfer through a non-Darcy porous medium channel with variable thermal conductivity and heat source effects," *Proceedings of the Institution of Mechanical Engineers, Part C*, vol. 223, no. 10, pp. 2341–2355, 2009.

[7] O. Anwar Bég, A. Y. Bakier, and V. R. Prasad, "Numerical study of free convection magnetohydrodynamic heat and mass transfer from a stretching surface to a saturated porous medium with Soret and Dufour effects," *Computational Materials Science*, vol. 46, no. 1, pp. 57–65, 2009.

[8] O. D. Makinde and O. Anwar Bég, "On inherent irreversibility in a reactive hydromagnetic channel flow," *Journal of Thermal Science*, vol. 19, no. 1, pp. 72–79, 2010.

[9] S. K. Ghosh, O. Anwar Bég, and M. Narahari, "Hall effects on MHD flow in a rotating system with heat transfer characteristics," *Meccanica*, vol. 44, no. 6, pp. 741–765, 2009.

[10] O. Anwar Bég, J. Zueco, R. Bhargava, and H. S. Takhar, "Magnetohydrodynamic convection flow from a sphere to a non-Darcian porous medium with heat generation or absorption effects: network simulation," *International Journal of Thermal Sciences*, vol. 48, no. 5, pp. 913–921, 2009.

[11] R. Bhargava, R. Sharma, and O. Anwar Bég, "A numerical solution for the effect of radiation on micropolar flow and heat transfer past a horizontal stretching sheet through porous medium," in *Proceedings of the 5th IASME/WSEAS International Conference on Continuum Mechanics (CM '10)*, University of Cambridge, Cambridge, UK, February 2010.

[12] O. Anwar Bég, A. Y. Bakier, V. R. Prasad, J. Zueco, and S. K. Ghosh, "Nonsimilar, laminar, steady, electrically-conducting forced convection liquid metal boundary layer flow with induced magnetic field effects," *International Journal of Thermal Sciences*, vol. 48, no. 8, pp. 1596–1606, 2009.

[13] O. D. Makinde, O. Anwar Bég, and H. S. Takhar, "Magnetohydrodynamic viscous flow in a rotating porous medium cylindrical annulus with an applied radial magnetic field," *Journal of Applied Mathematics and Mechanics*, vol. 5, no. 6, pp. 68–81, 2009.

[14] S. K. Ghosh, O. Anwar Bég, J. Zueco, and V. R. Prasad, "Transient hydromagnetic flow in a rotating channel permeated by an inclined magnetic field with magnetic induction

and Maxwell displacement current effects," *Zeitschrift fur Angewandte Mathematik und Physik*, vol. 61, no. 1, pp. 147–169, 2010.

[15] O. Anwar Bég, S. K. Ghosh, and M. Narahari, "Mathematical modeling of oscillatory MHD couette flow in a rotating highly permeable medium permeated by an oblique magnetic field," *Chemical Engineering Communications*, vol. 198, no. 2, pp. 235–254, 2011.

[16] N. Rudraiah, B. K. Ramaiah, and B. M. Rajasekhar, "Hartmann flow over a permeable bed," *International Journal of Engineering Science*, vol. 13, no. 1, pp. 1–24, 1975.

[17] O. Lioubashevski, E. Katz, and I. Willner, "Magnetic field effects on electrochemical processes: a theoretical hydrodynamic model," *Journal of Physical Chemistry B*, vol. 108, no. 18, pp. 5778–5784, 2004.

[18] N. G. B. Boum and A. Alemany, "Numerical simulations of electrochemical mass transfer in electromagnetically forced channel flows," *Electrochimica Acta*, vol. 44, no. 11, pp. 1749–1760, 1999.

[19] T. Z. Fahidy, "On the magnetohydrodynamics of natural convective diffusion boundary layers in coupled horizontal electric and magnetic fields," *Chemical Engineering Journal*, vol. 72, no. 1, pp. 79–82, 1999.

[20] M. A. Al-Nimr and M. A. Hader, "MHD free convection flow in open-ended vertical porous channels," *Chemical Engineering Science*, vol. 54, no. 12, pp. 1883–1889, 1999.

[21] J. D. McWhirter, M. E. Crawford, D. E. Klein, and T. L. Sanders, "Model for inertialess magnetohydrodynamic flow in packed beds," *Fusion Technology*, vol. 33, no. 1, pp. 22–30, 1998.

[22] S. K. Dahikar and R. L. Sonolikar, "Influence of magnetic field on the fluidization characteristics of circulating fluidized bed," *Chemical Engineering Journal*, vol. 117, no. 3, pp. 223–229, 2006.

[23] S. Alchaar, P. Vasseur, and E. Bilgen, "Effect of an electromagnetic field on natural convection in a porous medium," in *Proceedings of the 7th International Symposium on Transport Phenomena in Manufacturing Processes,*, pp. 275–280, Acapulco, Mexico, 1994.

[24] M. A. Mansour, M. A. El-Hakiem, and S. M. El Kabeir, "Heat and mass transfer in magnetohydrodynamic flow of micropolar fluid on a circular cylinder with uniform heat and mass flux," *Journal of Magnetism and Magnetic Materials*, vol. 220, no. 2, pp. 259–270, 2000.

[25] A. Postelnicu, "Influence of a magnetic field on heat and mass transfer by natural convection from vertical surfaces in porous media considering Soret and Dufour effects," *International Journal of Heat and Mass Transfer*, vol. 47, no. 6-7, pp. 1467–1472, 2004.

[26] O. Anwar Bég, R. Bhargava, S. Rawat, K. Halim, and H. S. Takhar, "Computational modeling of biomagnetic micropolar blood flow and heat transfer in a two-dimensional non-Darcian porous medium," *Meccanica*, vol. 43, no. 4, pp. 391–410, 2008.

[27] O. Anwar Bég, J. Zueco, and H. S. Takhar, "Laminar free convection from a continuously-moving vertical surface in thermally-stratified non-Darcian high-porosity medium: network numerical study," *International Communications in Heat and Mass Transfer*, vol. 35, no. 7, pp. 810–816, 2008.

[28] G. W. Sutton and A. S. Sherman, *Engineering Magnetohydrodynamics*, MacGraw-Hill, New York, NY, USA, 1965.

[29] S. I. Pai, *Magnetogasdynamics and Plasma Dynamics*, Springer, Berlin, Germany, 1962.

[30] W. F. Hughes and F. J. Young, *The Electromagnetodynamics of Fluids*, John Wiley & Sons, New York, NY, USA, 1966.

[31] H. B. Keller, "A new difference method for parabolic problems," in *Numerical Methods for Partial Differential Equations*, J. Bramble, Ed., 1970.

[32] T. Cebeci and P. Bradshaw, *Physical and Computational Aspects of Convective Heat Transfer*, Springer, New York, NY, USA, 1984.

[33] H. S. Takhar, O. Anwar Bég, and M. Kumari, "Computational analysis of coupled radiation-convection dissipative non-gray gas flow in a non-darcy porous medium using the keller-box implicit difference scheme," *International Journal of Energy Research*, vol. 22, no. 2, pp. 141–159, 1998.

[34] H. S. Takhar and O. Anwar Bég, "Effects of transverse magnetic field, prandtl number and reynolds number on non-darcy mixed convective flow of an incompressible viscous fluid past a porous vertical flat plate in a saturated porous medium," *International Journal of Energy Research*, vol. 21, no. 1, pp. 87–100, 1997.

[35] O. Anwar Bég, V. Prasad, H. S. Takhar, and V. M. Soundalgekar, "Thermoconvective flow in a saturated, isotropic, homogeneous porous medium using Brinkman's model: numerical study," *International Journal of Numerical Methods for Heat and Fluid Flow*, vol. 8, no. 5-6, pp. 559–589, 1998.

[36] H. S. Takhar, O. Anwar Bég, and M. Kumari, "Computational analysis of coupled radiation-convection dissipative non-gray gas flow in a non-darcy porous medium using the keller-box implicit difference scheme," *International Journal of Energy Research*, vol. 22, no. 2, pp. 141–159, 1998.

[37] A. J. Chamkha, H. S. Takhar, and O. Anwar Bég, "Radiative free convective non-newtonian fluid flow past a wedge embedded in a porous medium," *International Journal of Fluid Mechanics Research*, vol. 31, no. 2, pp. 101–115, 2004.

[38] O. Anwar Bég, H. S. Takhar, G. Nath, and M. Kumari, "Computational fluid dynamics modeling of buoyancy-induced viscoelastic flow in a porous medium under transverse magnetic field," *International Journal of Applied Mechanics and Engineering*, vol. 6, no. 1, pp. 187–210, 2001.

[39] V. Ramachandra Prasad, B. Vasu, and O. Anwar Bég, "Numerical modeling of transient dissipative radiation free convection heat and mass transfer from a non-isothermal cone with variable surface conditions," *Elixir-Applied Mathematics*, vol. 41, pp. 5592–5603, 2011.

[40] V. R. Prasad, B. Vasu, O. Anwar Bég, and R. D. Prashad, "Unsteady free convection heat and mass transfer in a Walters-B viscoelastic flow past a semi-infinite vertical plate: a numerical study," *Thermal Science*, vol. 15, no. 2, supplement, pp. S291–S305, 2011.

[41] V. R. Prasad, B. Vasu, O. Anwar Bég, and D. R. Parshad, "Thermal radiation effects on magnetohydrodynamic free convection heat and mass transfer from a sphere in a variable porosity regime," *Communications in Nonlinear Science and Numerical Simulation*, vol. 17, no. 2, pp. 654–671, 2012.

[42] K. Vafai and C. L. Tien, "Boundary and inertia effects on convective mass transfer in porous media," *International Journal of Heat and Mass Transfer*, vol. 25, no. 8, pp. 1183–1190, 1982.

[43] J. Bear, *Dynamics of Fluids in Porous Media*, Dover, New York, NY, USA, 1988.

[44] H. Belhaj, J. Biazar, S. Butt, and R. Islam, "Adomian solution of Forchheimer model to describe porous media flow," in *Proceedings of the SPE/DOE Symposium on Improved Oil Recovery*, Tulsa, Okla, USA, April 2004.

[45] S. Whitaker, "The Forchheimer equation: a theoretical development," *Transport in Porous Media*, vol. 25, no. 1, pp. 27–61, 1996.

[46] Y. Qin and J. Chadam, "Nonlinear convective stability in a porous medium with temperature-dependent viscosity and inertial drag," *Studies in Applied Mathematics*, vol. 96, no. 3, pp. 273–288, 1996.

[47] H. Schlichting, *Boundary-Layer Theory*, MacGraw-Hill, New York, NY, USA, 8th edition, 2000.